Improving positively tuned voltage indicators for brightness and kinetics

Sungmoo Lee[1,10], Guofeng Zhang[1,9,10], Laura C. Gomez[2,3], Guilherme Testa-Silva[4], Yukun Alex Hao[1,5], Atsuki Hiramoto[4], Dongyun Jiang[1], Richard H. Roth[6], Jun Ding[6], Thomas R. Clandinin[1], Botond Roska[4,7], Daniel Feldman[2], Na Ji[2,3], and Michael Z. Lin[1,5,8]

Affiliations
1, Department of Neurobiology, Stanford University, Stanford, CA 94305, USA
2, Department of Molecular and Cell Biology and Helen Wills Neuroscience Institute, University of California Berkeley, Berkeley, CA, 94720, USA
3, Department of Physics, University of California, Berkeley, CA, 94720, USA
4, Institute of Molecular and Clinical Ophthalmology Basel, 4031 Basel, Switzerland
5, Department of Bioengineering, Stanford University, Stanford, CA 94305, USA
6, Department of Neurosurgery, Stanford University, Stanford, CA 94305, USA
7, Department of Ophthalmology, University of Basel, 4001 Basel, Switzerland
8, Correspondence: mzlin@stanford.edu
9, Current Address: Department of Neurosurgery, The First Affiliated Hospital, Sun Yat-sen University, Guangzhou, Guangdong, 510080, China
10, Equal contribution

ABSTRACT

The recent positively tuned ASAP4-family voltage indicators feature superior photostability compared to the negatively tuned ASAP3, but signal-to-noise ratios (SNRs) for spike detection were not significantly different. To improve spike detection by positively tuned ASAP indicators, we performed multiple rounds of structure-guided saturation mutagenesis of an ASAP4 template while screening directly for faster responses. Our resulting variants, ASAP6.1 and ASAP6b, demonstrated sufficient dynamic range and kinetics, and reported action potentials *in vivo* by one-photon and two-photon microscopy with high SNR and temporal resolution.

Previously, we developed positively tuned ASAP4-subfamily GEVIs with high photostability[1]. While these had higher $\Delta F/F_0$ from –70 mV to +30 mV than the negatively tuned ASAP3[2] or ASAP5, their F-V curves were spread out over a larger voltage range. In addition, ASAP4b and ASAP4e onset kinetics are biexponential with only a minority component of the response exhibiting a time constant of < 10 ms. Both limitations could be due to steric or electrostatic interactions that cause resistance to upward S4 movement in ASAP4 variants. Thus, we set out to engineer positively tuned GEVIs with faster activation kinetics over ASAP4b and ASAP4e, while maintaining or improving steady-state responsivity.

Engineering positively tuned ASAPs for larger responsivity for action potentials

As ASAP4 and ASAP3 differ primarily in linker sequences, we rescreened ASAP4.0, a precursor to ASAP4b and ASAP4e, performing double-site saturation mutagenesis (400 amino acid combinations) at pairs of sites selected from the chromophore-adjacent residues Phe-148, Asn-149, Asp-150, Gly-151, and His-206 (**Fig. 1a, Supplementary Note**). This identified ASAP4.0 G151K T206A as similar in responsivity to the previously reported ASAP4.0 T206H (ASAP4.1)[1] (**Supplementary Fig. 1)**. In a second round, screening of Asn-149 mutants by electroporation (**Supplementary Fig. 2**) and patch-clamping then found the largest predicted SNRs to single APs in ASAP4.0 N149K T206H and ASAP4.0 N149A G151K T206A **(Supplementary Fig. 3)**

For a third round of mutagenesis, we turned our attention to the voltage-sensing domain (VSD). In ASAP2s[3], a R414Q mutation caused larger steady-state responses but slower kinetics. The deceleration could be explained by R414 being a gating charge, and VSDs with more gating charges generally exhibit faster VSD movements, which can be explained by electrostatic force on S4 being greater with more gating charges[4]. In addition, the adjacent side chain at amino acid 413 at the interface between the lipid bilayer and the cytosol was found to be critical for F-V tuning in ASAP4.3–4.5. We thus generated and screened all 400 combinations of mutations at positions 413 and 414 in ASAP4.0 N149K

T206H and ASAP4.0 N149A G151K T206A (**Supplementary Fig. 4**). By increasing the imaging frame rate of our automated electroporation screening system to 300 frames-per-second (fps), we could obtain useful information on kinetics as well as steady-state responses from the same image series in the primary screen. To avoid being trapped in a local performance minimum specific to the second-round choice at Asn-149, we also performed F413X Q414X mutagenesis on the first-round hits ASAP4.0 T206H and ASAP4.0 G151K T206A (**Supplementary Fig. 5**). We then performed patch-clamp verification on the top 5-10 variants with better response and at least comparable kinetics to the parent template.

These four third-round screens revealed two interesting mutants. One, ASAP6.1, had the largest relative response per AP **(Supplementary Table 1**). Another, ASAP6.2, had the best per-molecule SNR for APs due to operating in a brighter range (**Supplementary Table 1)**. ASAP6.1 and ASAP6.2 exhibited mono-exponential time constants of 4.0 and 3.7 ms, respectively (**Table 1**). As a single ≤4-ms time constant now accounts for 100% of the onset kinetics, as opposed to only 14% for the similar tau1 in ASAP4e, these mutants should achieve improved responses to APs.

Improved responses of ASAP6 for spike waveforms

We further characterized ASAP 6.1 and 6.2. The maximum-normalized fluorescence-voltage (F-V) curves showed the ASAP6.2 input range to be shifted to more negative voltages and thus to operate at higher molecular brightness in physiological conditions **(Fig. 1b)**. We thus named ASAP6.2 as ASAP6b for its higher brightness. Responses to AP-like waveforms with 2-ms full-width at half maximum (FWHM) reached 50% for ASAP6.1 and 33% for ASAP6b, compared to 23% for ASAP4e in HEK293 cells at room-temperature (**Fig. 1c**). In cultured neurons injected with current to elicit action potentials, both ASAP6.1 and ASAP6b faithfully recapitulated spike dynamics with sufficient SNR for spike trains as fast as 30Hz in frequency (**Fig. 1d**).

Detecting spiking activity *ex vivo* and *in vivo*

We performed 1P voltage imaging in murine whole-mount retinal explants. Both ASAP6.1-Kv and ASAP6b-Kv reliably displayed spontaneous action potentials from retinal ganglion cells (RGCs) (**Fig. 2a–2c**). In this example, we could confirm a good membrane localization of virally introduced ASAP6b-Kv in RGCs (**Fig. 2d**).

Then we set out to test the new variants in the mouse brain using a simple widefield epi-fluorescence microscope. From sparsely labeled pyramidal neurons in layer 2/3 of the primary motor cortex, both sensors successfully showed spiking activity with high SNR from awake-behaving mice (**Fig. 3a**).

Next, we tested the 2P performance of ASAP6b-Kv in the mouse barrel cortex under the conventional resonant-Galvo scanning microscope (**Fig. 3b**). In response to a whisker-stimulation, ASAP6b-Kv clearly visualized spikes from the neurons located at layer 2/3. Simultaneous imaging of a red-shifted calcium indicator, jRGECO1a[5], was unable to reveal the individual spikes reliably. Also, jRGECO1a signals did not return to baseline with the same time course as voltage, consistent with the slow off-kinetics of calcium transients[6, 7]. Together, these examples demonstrate the utilities of the two ASAP6 variants in different preparations under both 1P and 2P microscope setups.

In this preprint, we introduce improved versions of positively tuned ASAP-family GEVIs engineered by saturation mutagenesis of rationally selected amino acid combinations at the interface of the fluorescent protein and the VSD, and the residues near the gating charges. The faster onset kinetics of the two ASAP6 variants enable larger $\Delta F/F_0$ for suprathreshold neuronal activity compared to the previously reported positively tuned ASAP family, ASAP4b and ASAP4e[1]. We show that ASAP6.1 and ASAP6b can detect fast spiking activities with 1P and 2P epi-fluorescence microscopes in *in vitro, ex vivo* and *in vivo* preparations. Simultaneous voltage and calcium imaging in the mouse barrel cortex shows a substantially larger response of ASAP6b-Kv for individual spikes compared to a red-shifted calcium indicator, jRGECO1a.

With a dimmer baseline fluorescence than the negatively tuned GEVIs such as ASAP3[2], JEDI2P[8], or the recently developed ASAP5 (manuscript in preparation), ASAP6.1 and ASAP6b are still not preferred for subthreshold voltage changes, where the molecular brightness of the indicator remains near the baseline. However, ASAP6.1 and ASAP6b are well suited for extended-duration detection of action

potentials. In fact, simulations[9] suggest that a positively tuned GEVI with > 40% peak $\Delta F/F_0$ may achieve more accurate spike detection at a labeling density higher than 200cells / mm^2 compared to the negatively tuned GEVIs with brighter baseline fluorescence. Unlike the previous positively tuned ASAPs[1], ASAP6.1 and ASAP6b now show large responsivity for spiking activity *in vivo* (**Fig. 3**). Therefore, we expect the two ASAP6 variants can achieve 1P widefield voltage imaging from a population of densely labeled neurons as it is routinely done by using calcium indicators[10-12].

Declaration of interests

M.Z.L. is an inventor on a patent for the earlier ASAP1 voltage indicator. The remaining authors declare no competing interests.

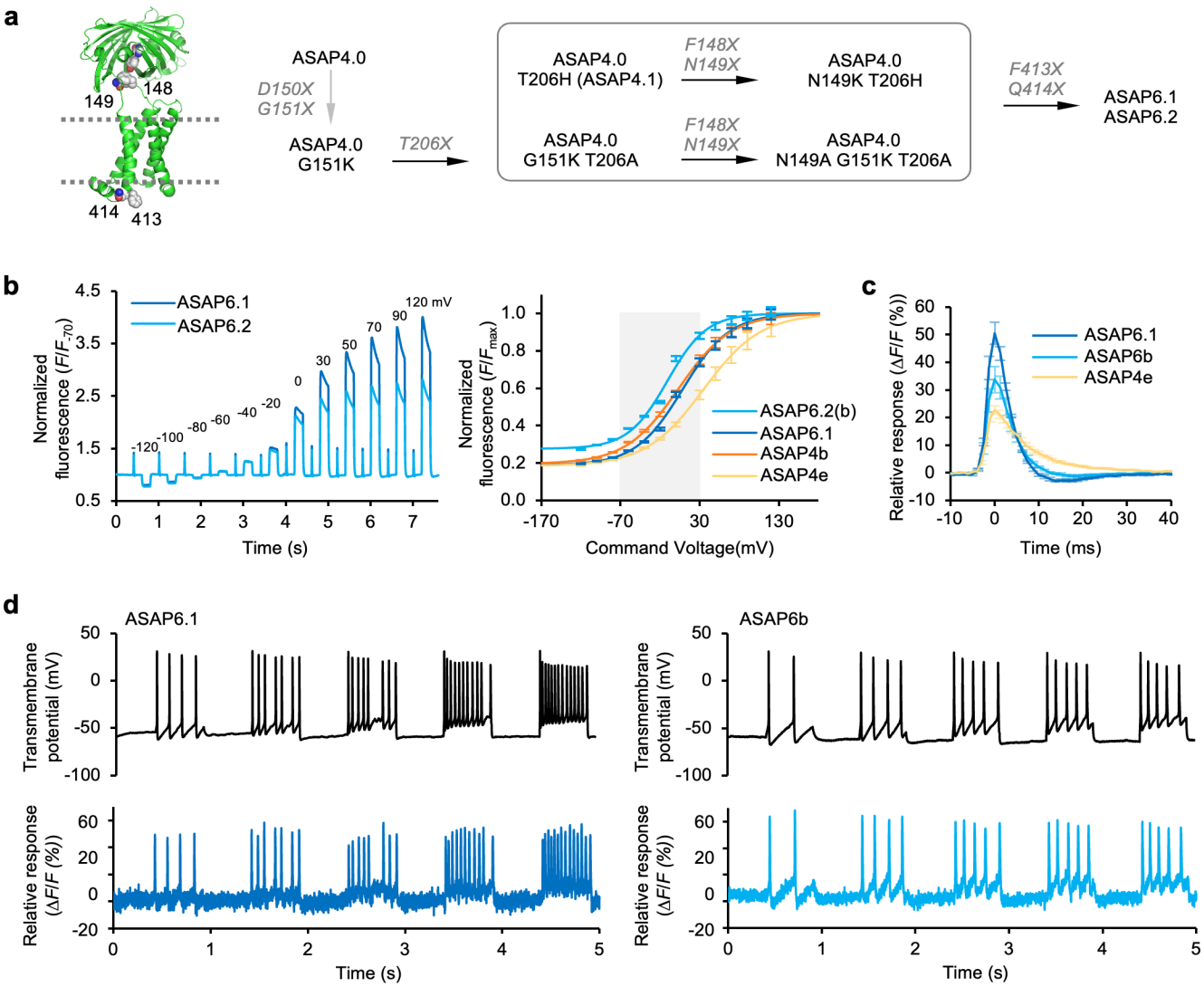

Figure 1. Protein engineering and *in vitro* characterization of ASAP6

a. Left, ASAP4.1 protein model showing mutated positions. The engineered residues and the chromophore are highlighted as spheres. Right, the engineering paths for ASAP6.1 and ASAP6.2.

b. Left, representative steady-state responses to voltage commands in HEK293A cells for ASAP6.1 and ASAP6.2 (6b) normalized to their fluorescence signals at -70mV. Right, resulting F–V curves normalized to the maximum $\Delta F/F$ signal for each sensor. Error bars represent standard error of the mean (SEM). N = 7, 8, 6, 6 for ASAP6.2(b), ASAP6.1, ASAP4b, and ASAP4e, respectively.

c. Mean fluorescence responses to simulated AP-shaped waveform with 2ms half-width in HEK293A cells. The AP-shaped waveform was used as a command voltage in whole-cell voltage clamp mode. Error bars represent SEM. N = 4, 4, and 5 for ASAP6.1, ASAP6b, and ASAP4e, respectively.

d. Example traces of action potentials evoked by current injection in cultured rat hippocampal neurons. The fluorescence traces were acquired at 877Hz (left, ASAP6.1) and 800Hz (right, ASAP6b) frame rates.

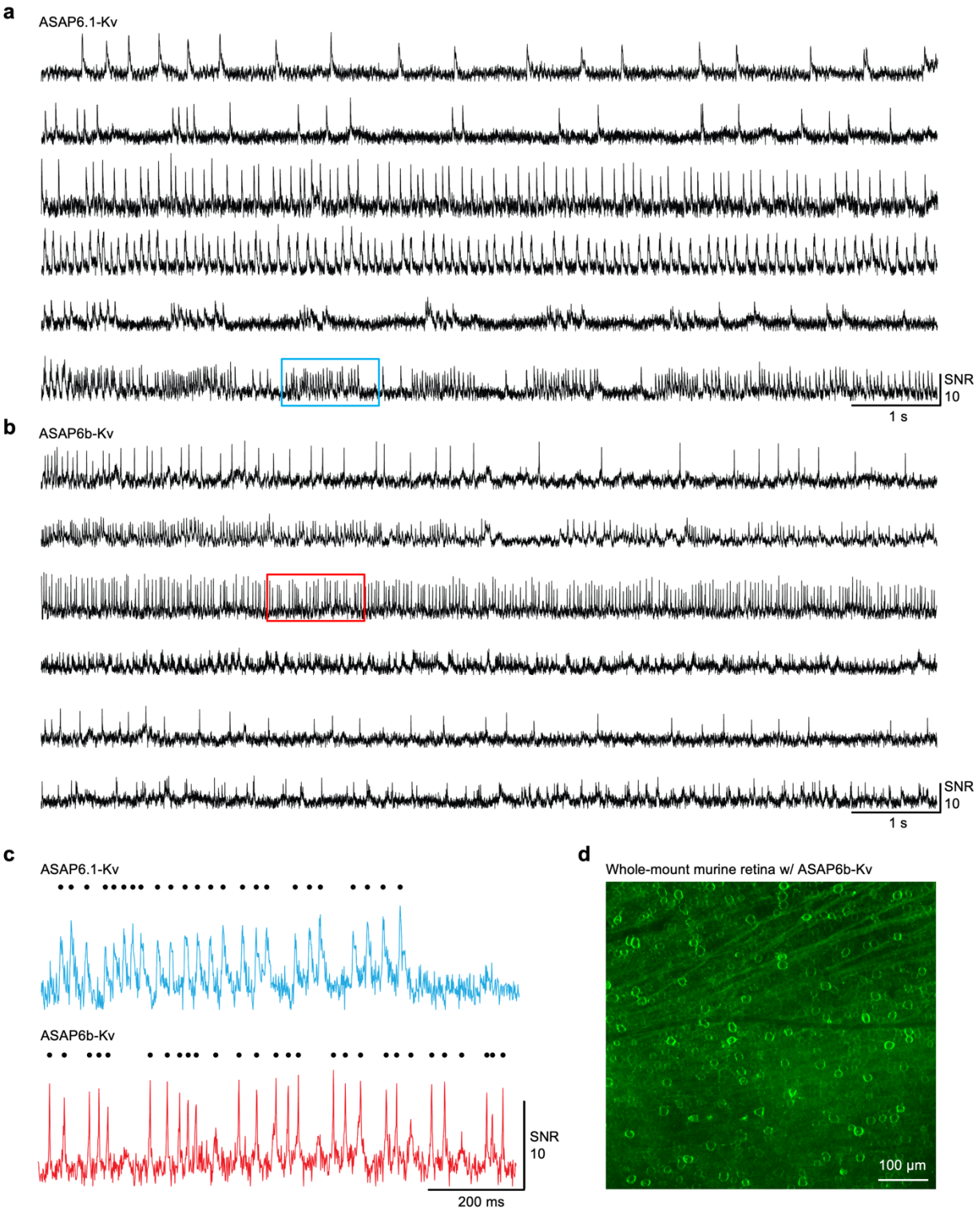

Figure 2. One-photon voltage imaging of ASAP6.1 and ASAP6b in retina.
a-b. Voltage imaging of spontaneously firing spikes from mouse retinal ganglion cells expressing ASAP6.1-Kv (a) or ASAP6b-Kv (b) under the hSyn promoter.
c. Fluorescence traces showing zoomed-in traces of either ASAP6.1-Kv (blue) or ASAP6b-Kv (red) from the insets of a and b, respectively.
d. A fluorescence image of a whole-mount mouse retinal explant expressing ASAP6b-Kv.

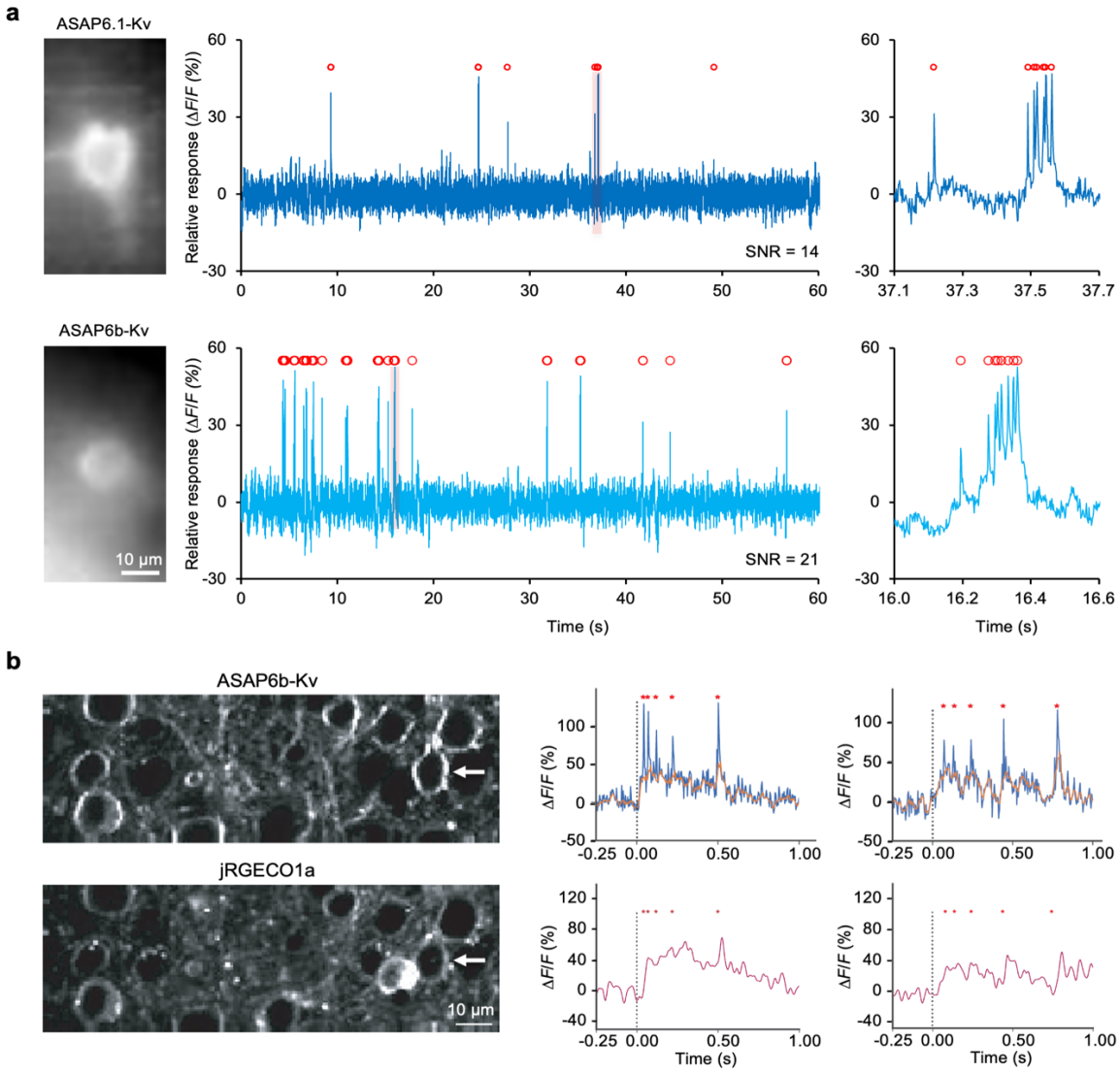

Figure 3. One-photon and two-photon voltage imaging in the cortex

a. Left, One-photon fluorescence images of ASAP6.1-Kv (upper panel) and ASAP6b-Kv (lower panel) expressing neurons. The images were averaged over 1-min. Middle, Example fluorescence traces from the neurons shown on the left. Red circles indicate optical spikes detected by a spike-detection algorithm, VolPy. The SNRs were averaged from 14 spikes for ASAP6.1-Kv, and 86 spikes for ASAP6b-Kv. Right, Zoomed-in traces of the time window shaded in red from the traces in the middle. Both images were acquired at 500Hz. The irradiance was 40–50mW / mm^2.

b. Left, Two-photon excited fluorescence images acquired from a mouse expressing both ASAP6.2-Kv (upper panel) and jRGECO1a (lower panel) in the barrel cortex. The arrows indicate the neuron analyzed. Right, resulting fluorescence traces of either voltage imaging (upper panels) or calcium imaging (lower panels) in two different stimulus trials. The dotted lines represent the timing of whisker-stimulation. The asterisks in red indicate spikes detected by VolPy. The orange-colored traces for the upper panels represent low-pass filtered slow oscillations.

Time constants (ms)	ASAP6.1	ASAP6.2 (6b)
Depolarization (-70 to +30 mV)	3.99 ± 0.20	3.74 ± 0.26
Repolarization (+30 to -70 mV)	4.89 ± 0.11	6.16 ± 0.13

Table 1. Kinetics measured at room-temperature in HEK293A cells imaged at 800Hz.

	V_{half} [a]	Per-molecule fluorescence at –70 mV	Per-molecule fluorescence at +30 mV	Per-molecule fluorescence change, 100 mV	Relative fluorescence change, 100 mV	Per-molecule fluorescence change, 1 AP	Relative fluorescence change, 1 AP [b]	Per-molecule SNR determinant, 1 AP	Relative fluorescence ratio, 1 AP per 100mV fluorescence change [c]
	(mV)	($mF_0 = F_{-70}/F_{max}$)	(F_{+30}/F_{max})	($m\Delta F = \Delta F_{100}/F_{max}$)	($m\Delta F/mF_0$, %)	($m\Delta F_{AP}$, %)	($m\Delta F_{AP}/mF_0$, %)	($m\Delta F_{AP}/mF_0^{1/2}$)	($m\Delta F_{AP}/m\Delta F$)
ASAP4.0	40.41	0.24	0.54	0.30	127	6	25	0.12	0.20
ASAP4.1 (=ASAP4.0 T206H)	-10.85	0.44	0.87	0.43	96	11	25	0.17	0.26
ASAP4.2 =ASAP4.1 F148P N149V	-16.65	0.42	0.83	0.41	97	10	24	0.16	0.25
ASAP4.1 F148A N149V	35.52	0.22	0.52	0.30	133	5	23	0.11	0.17
ASAP4.1 F148D N149V	-18.99	0.45	0.81	0.36	81	10	22	0.15	0.27
ASAP4.1 F148I N149V	33.57	0.16	0.53	0.37	231	6	35	0.14	0.15
ASAP4.1 F148L N149V	16.2	0.24	0.66	0.42	175	7	28	0.14	0.16
ASAP4.1 F148F N149K	-33.38	0.49	0.89	0.40	80	16	33	0.23	0.41
ASAP4b	3.24	0.28	0.75	0.47	168	9	31	0.16	0.18
ASAP4e	35.82	0.17	0.53	0.36	212	6	33	0.14	0.16
ASAP4.0 G151K	22.04	0.20	0.57	0.37	185	7	33	0.15	0.18
ASAP4.0 G151K T206A	-13.47	0.32	0.79	0.47	145	10	32	0.18	0.22
ASAP4.0 G151K T206A F148F N149A	-48.32	0.49	0.93	0.44	89	15	31	0.22	0.35
ASAP4.0 G151K T206A F148F N149D	-41.4	0.48	0.90	0.43	90	15	31	0.21	0.34
ASAP4.0 G151K T206A F148F N149P	-16.87	0.32	0.82	0.50	154	7	21	0.12	0.14
ASAP6.1	8.61	0.24	0.73	0.49	204	15	63	0.31	0.31
ASAP6.2 (6b)	-10.83	0.34	0.88	0.54	161	19	56	0.33	0.35

a. Midpoint of F-V curve fit to Boltzmann function.
b. $\Delta F/F_0$ fluorescence change per AP waveform(FWHM = 3.5ms, amplitude = 100mV) by voltage patch-clamp in HEK293A cells at room temperature.
c. Ratio of per-molecule fluorescence change per AP waveform(FWHM = 3.5ms, amplitude = 100mV) and per voltage command step(from -70mV to +30mV).

Supplementary table 1. Summary of ASAP4.1 and ASAP4.0 G151K T206A engineering as well as ASAP6.1 and ASAP6.2**.**

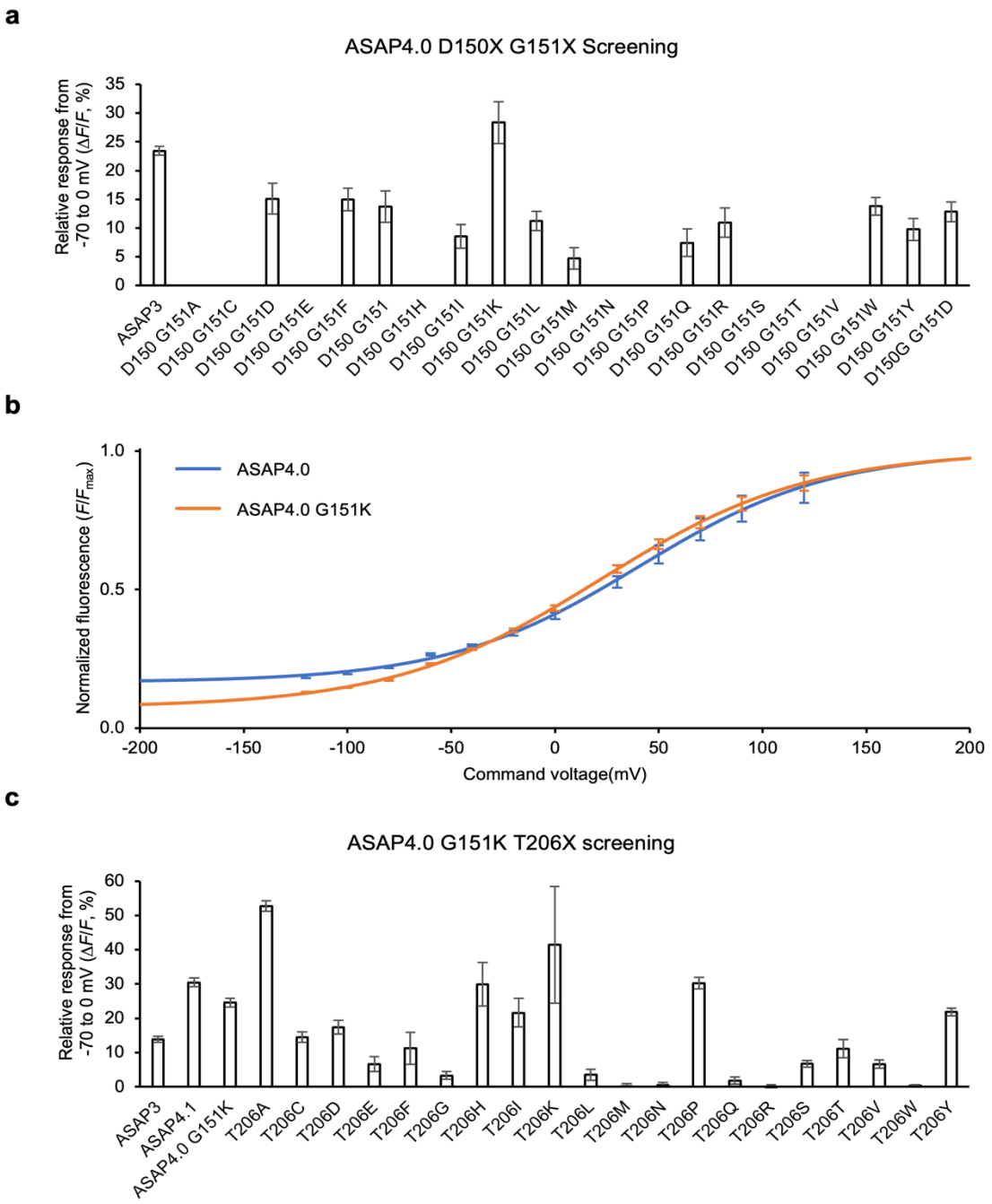

Supplementary figure 1. Screening G151X and T206X of ASAP4.0 yielded ASAP4.0 G151K T206A.
a. Peak $\Delta F/F$ responses upon electroporation of HEK293-Kir2.1 cells transfected with PCR fragment library for screening ASAP4.0 D150 G151X variants. ASAP4.0 D150 G151K showed the largest response. Error bars are SEM.
b. Resulting F–V curves of ASAP4.0 and ASAP4.0 G151K normalized to F_{max} values. Error bars are SEM. N = 5 (ASAP4.0) and 11 (ASAP4.0 G151K).
c. Peak $\Delta F/F$ responses upon electroporation of HEK293-Kir2.1 cells transfected with PCR fragment library for screening ASAP4.0 G151K T206X variants resulted in ASAP4.0 G151K T206A. Error bars are SEM.

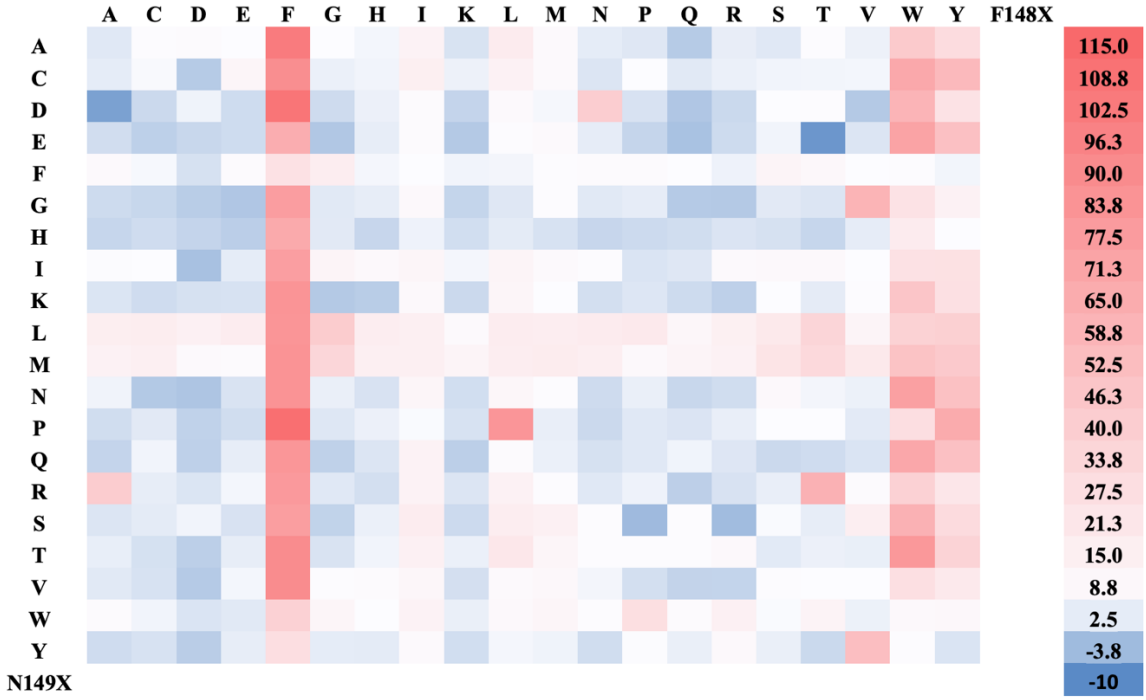

Supplementary figure 2. Screening result of a double-site saturation mutagenesis library of ASAP4.0 G151K T206A F148X N149X. The blue-to-red color scale represents the $\Delta F/F$ (%) response upon electroporation of HEK293-Kir2.1 cells experiencing approximately -70mV to 0mV membrane depolarization.

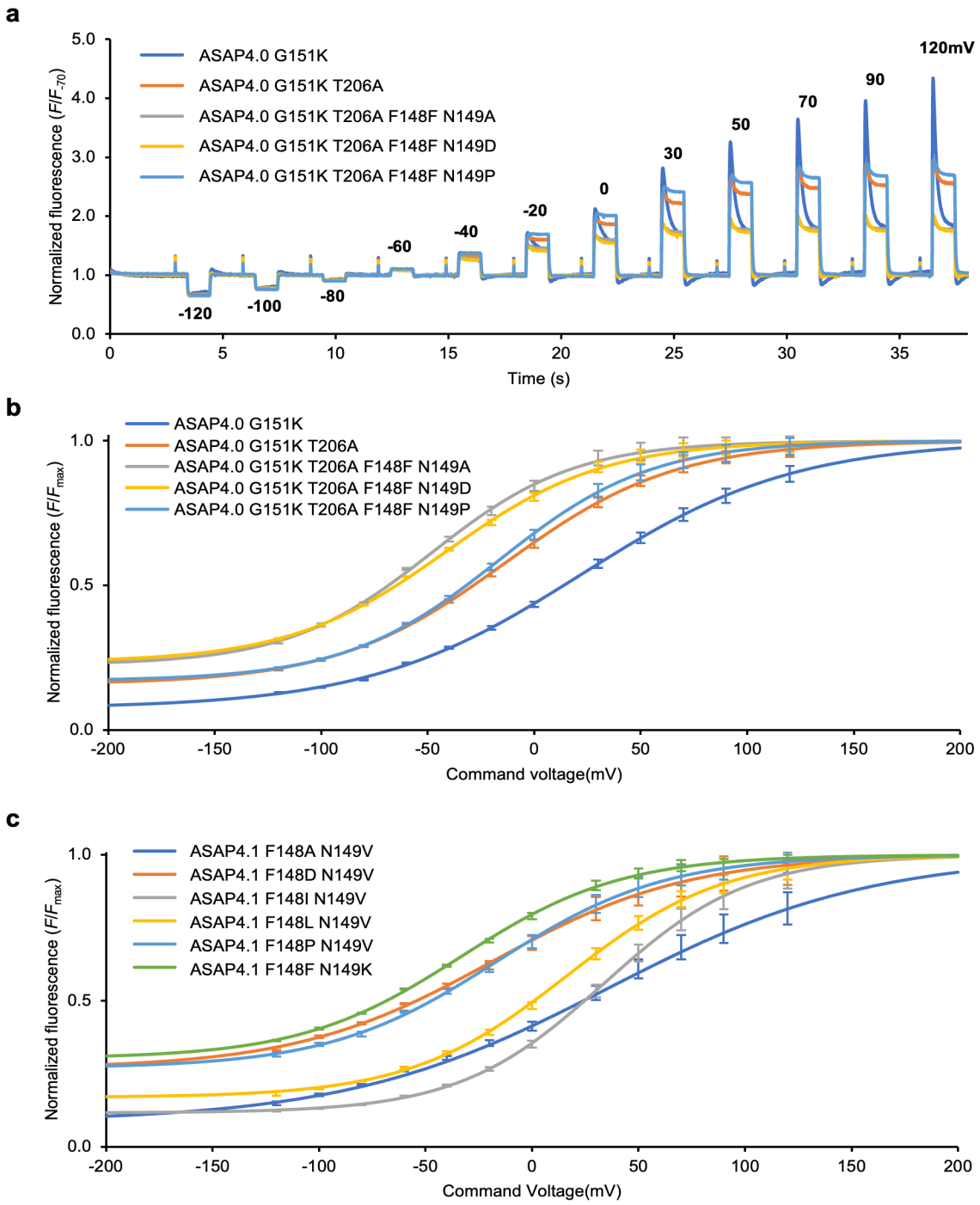

Supplementary figure S3. Steady-state responses of selected variants from ASAP4.0 G151K T206A F148X N149X and ASAP4.1 F148X N149X screening.

a. Representative responses of HEK293A cells expressing ASAP4.0 G151K and four variants of ASAP4.0 G151K T206A F148X N149X. The cells were patched in whole-cell voltage clamp mode with command voltage steps.

b. Resulting F–V curves of a. normalized to F_{max} values. Error bars are SEM. N = 11 (ASAP4.0 G151K), 5 (ASAP4.0 G151K T206A), 5 (ASAP4.0 G151K T206A F148F N149A), 5 (ASAP4.0 G151K T206A F148F N149D), and 6 (ASAP4.0 G151K T206A F148F N149P).

c. F–V curves of six variants of ASAP4.1 F148X N149X normalized to F_{max} values. Error bars are SEM. N = 6 (ASAP4.1 F148A N149V), 6 (ASAP4.1 F148D N149V), 3 (ASAP4.1 F148I N149V), 3 (ASAP4.1 F148L N149V), 6 (ASAP4.1 F148P N149V), and 6 (ASAP4.1 F148F N149K).

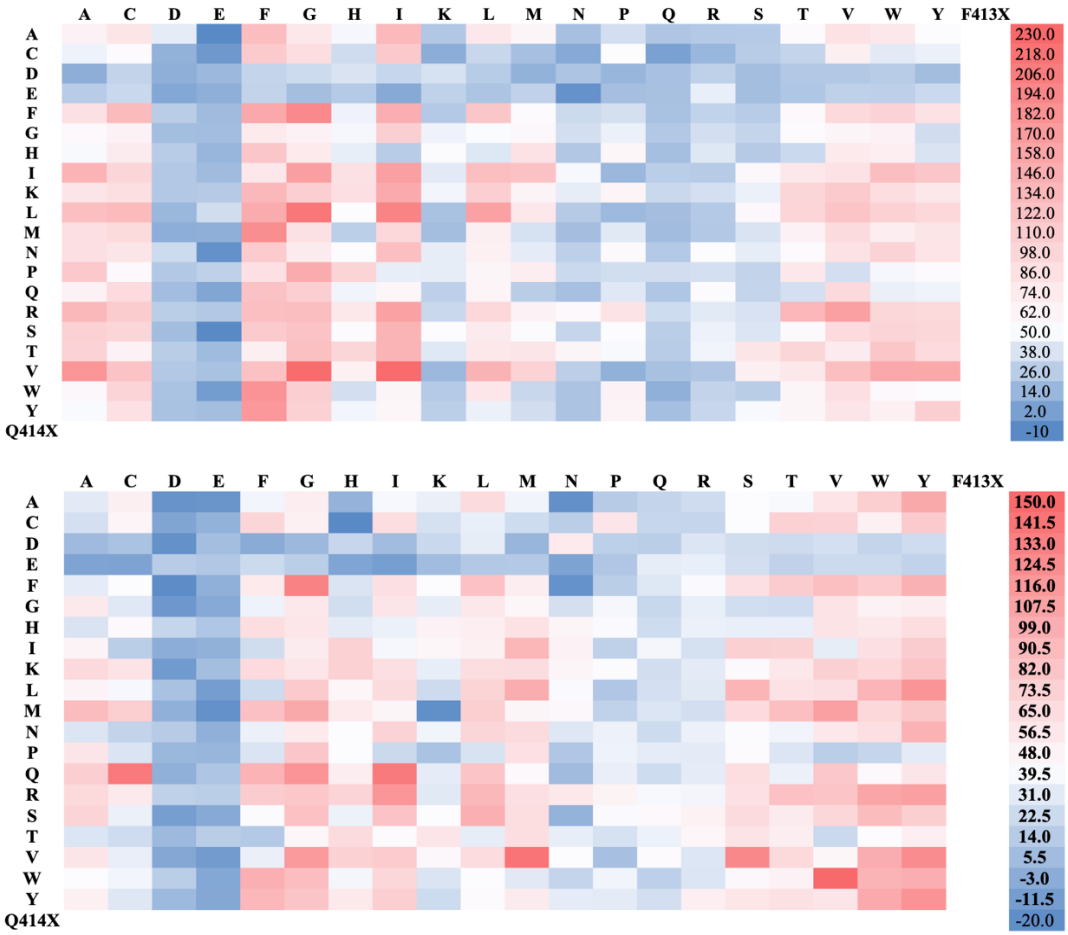

Supplementary figure 4. Screening results of double-site saturation mutagenesis library of ASAP4.0 N149K T206H F413X Q414X (upper panel) and ASAP4.0 N149A G151K T206A F413X Q414X (lower panel) expressing HEK293-Kir2.1 cells. The blue-to-red color scale represents the $\Delta F/F$ (%) response upon electroporation of HEK293-Kir2.1 cells experiencing approximately -70mV to 0mV membrane depolarization.

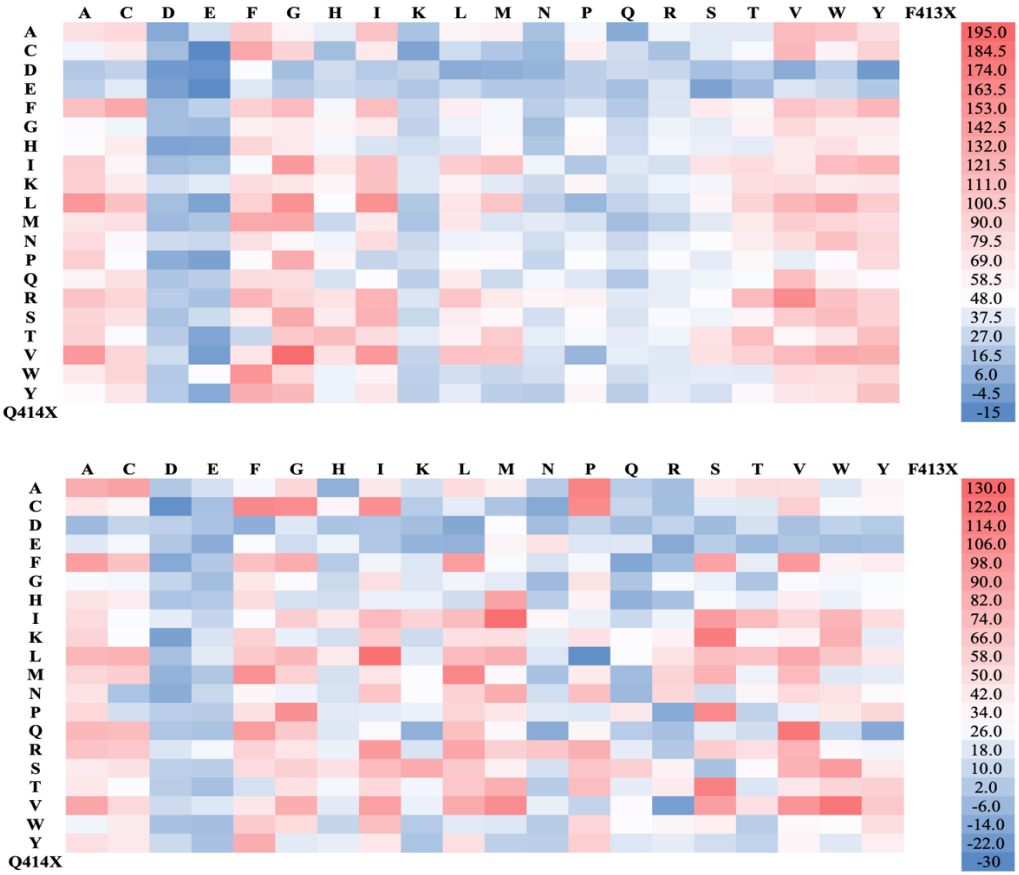

Supplementary figure 5. Screening results of double-site saturation mutagenesis library of ASAP4.0 T206H F413X Q414X (upper panel) and ASAP4.0 G151K T206A F413X Q414X (lower panel) expressing HEK293-Kir2.1 cells. The blue-to-red color scale represents the $\Delta F/F$ (%) response upon electroporation of HEK293-Kir2.1 cells experiencing approximately -70mV to 0mV membrane depolarization.

Supplementary Note

We initially concentrated on a series of variants with D150X G151X mutations relative to ASAP4.0, as these sites seemed to tolerate multiple amino acids in the screening that led to ASAP4.0[1]. We found ASAP4.0 G151K to have a better responsivity in the electroporation screening and upon voltage-clamp testing **(Supplementary Fig. 1a-1b**), driving a large SNR determinant for AP detection (relative response to a commanded AP waveform multiplied by the square root of basal brightness, **Supplementary Table 1**). We performed screening of T206X mutants on ASAP4.0 G151K, analogous to the mutagenesis of ASAP4.0 that yielded T206H to create ASAP4.1. In ASAP4.0 G151K, T206A stood out with the largest responsivity (**Supplementary Fig. 1c**), in contrast to T206H in ASAP4.1.

Retracing the evolutionary process from ASAP4.1 to ASAP4.2 by yet another step, we used ASAP4.0 G151K T206A as a template for F148X N149X saturated double site mutagenesis. We found three similar variants keeping Phe-148 but with Ala, Asp, or Pro at 149 pointing to the chromophore **(Supplementary Fig. 2-3)**. Among these, ASAP4.0 N149A G151K T206A showed the best SNR determinant on simulated APs **(Supplementary Fig. 3a-b, Supplementary Table 1)**. Since the N149A mutation was beneficial in ASAP4.0 G151K T206A without any change to F148, we also re-examined by patch-clamping F148F N149X library isolated from the published ASAP4.0 T206H F148X N149X screen (**Supplementary Fig. 3c**). We found ASAP4.0 N149K T206H to have brighter baseline fluorescence, larger responsivity, and faster kinetics than the previous ASAP4.2, resulting in a higher SNR determinant for APs (**Supplementary Table 1**). This supplied ASAP4.0 N149K T206H and ASAP4.0 N149A G151K T206A as two leads for the kinetic screen.

METHODS

Sensor engineering and *in vitro* characterization

Plasmid Construction

For electroporation-based screening transfection into HEK293-Kir2.1 Cells for electrical screening, ASAP variants were subcloned into pcDNA3.1 with a CMV enhancer and promoter and bGH poly(A) signal. All plasmids were made by standard molecular biology techniques followed by a Sanger sequencing (Sequetech). PCR fragment libraries were generated using standard PCR techniques, which were used to directly transfect HEK293-Kir2.1 cells with the linear product using lipofectamine 3000 (Thermo Fisher Scientific). For characterization in HEK293A cells, all voltage indicator variants were subcloned into a pcDNA3.1/Puro-CAG vector [13].

For *in vitro* characterization in cultured neurons, ASAP variants were subcloned into pAAV.hSyn.WPRE vector. The soma-targeting tag from Kv2.1 was used as previously described[2, 14] for restricting ASAP expression in soma and proximal dendrites.

Cell Lines

All cell lines were maintained in a humidified incubator at 37°C with 5% CO_2. For electroporation-based screening, HEK293-Kir2.1 cell line was maintained in high-glucose DMEM, 5% FBS, 2 mM L-glutamine, and 500 µg/mL Geneticin (Life Technologies) as previously described[2]. For patch-clamp recordings for *in vitro* characterization, HEK293A cells were used and cultured in the same DMEM based media as described above but without adding Geneticin.

Primary Neuronal Culture and Transfection

Hippocampal neurons were isolated from the Hippocampi of embryonic day 17–18 Sprague Dawley rats by dissociating in TrypLE™ Select Enzyme (Gibco) supplemented with 0.005% DNaseI in an incubator maintained at 37°C and 5% CO_2. The dissociated neurons were plated on poly-D-lysine coated 12 mm diameter glass coverslips at a density of 4 x 10^4 cells/cm_2. Cells were plated for several hours in Neurobasal media (Gibco) with 10% v/v FBS (Gemini bio), 2mM GlutaMAX (Gibco), and 5% v/v B27 supplement (Gibco), then the media were replaced with Neurobasal media supplemented with 1% FBS, 2mM GlutaMAX, and B27. A half of the media in each well was replaced every 3–4 days with fresh Neurobasal media supplemented with the same GlutaMAX and B-27, but without FBS. 5-Fluoro-2'-deoxyuridine (Sigma-Aldrich) was typically added at a final concentration of 16 uM at DIV 7–9 to limit non-neuronal cell growth. On DIV 9–11, Hippocampal neurons were transfected using a modified Lipofectamine 2000 (Life Technologies) transfection procedure as previously described [1]

Viruses

All ASAP viruses were produced by the Stanford Neuroscience Gene Vector and Virus Core facility at Stanford University.

High-throughput Automated Electroporation-based Cell Screening

Electroporation-based cell screening was conducted following the procedure as previously described[1]. Briefly, HEK293-Kir2.1 cells were plated in 384-well bottomless adhesive plates (Grace Bio-Labs) attached with an indium tin oxide coated conductive glass slides (Delta Technologies). Poly-D-lysine hydrobromide (MP biomedicals) was coated before plating the cells. ASAP mutation libraries were PCR fragments with a CMV enhancer and promoter at 5' end and bGH poly(A) signal at 3' end. Cells were transfected with either plasmid controls or PCR fragment libraries in 384-well plates with Lipofectamine 3000 (~100 ng plasmid DNA or equivalent transfection efficiency of PCR fragments, 0.4 µL p3000 reagent, 0.4 µL Lipofectamine per well) followed by a media change 4–5 hours later. The screening was done 2 days post-transfection in Hank's Balanced Salt solution (HBSS) buffered with 10 mM HEPES (Life Technologies). Cells were imaged at room temperature on an IX-81 inverted microscope using a 20x

0.75-numerical aperture (NA) objective lens (all Olympus). A 120-W metal halide lamp (X-Cite 120PC, Exfo) served as the excitation light source. The filter cube set consisted of a 480/40nm excitation filter and a 503-nm long pass emission filter. During the screening, an operator located the best field-of-view (FOV) and the focus for each well. A single FOV per well was imaged for a total of 3 s, with a 10-μs 150-V square pulse applied near the 1-s mark. The fluorescence was collected at 300 Hz (3.3-ms exposure time per frame) by an ORCA Flash4.0 V2 C11440–22CA sCMOS camera (Hamamatsu) with the FOV cropped to 512 x 170 pixels (binned 4-by-4). Each mutant had at least 4 replicates.

Whole Cell Patch Clamping and Imaging of HEK293A Cells

Patch-clamp experiments were conducted as previously described[1]. Briefly, the transfected HEK293A cells were replated on 12 mm diameter glass coverslips (Carolina Biological), and each coverslip was located in a patch chamber after 24 hours of transfection. Following a successful giga-ohm seal with a patch pipette with 3-5 MΩ resistance, the cell was patched in a whole-cell voltage-clamp mode with a Multiclamp 700B amplifier controlled by pClamp software (Molecular Devices). Fluorophores were illuminated with UHP-F-455 LED (Prizmatix) passed through a 484/15-nm excitation filter (Chroma) and focused on the sample through a 40x 1.3-NA oil-immersion objective (Zeiss). Emitted fluorescence passed through a 525/50-nm emission filter (Semrock) and was captured by an iXon 860 electron-multiplying charge-coupled device camera (Oxford Instruments) cooled to maintain -80°C. For all experiments fluorescence traces were corrected for photobleaching by dividing the recorded signal by an exponential fit to the data. To characterize steady-state fluorescence responses, cells were voltage-clamped at a holding potential of –70 mV, then voltage steps of 1 s duration between -120 and +120 mV were imposed. To obtain complete voltage-tuning curves, voltage steps from -200 to +120 mV were used. When the membrane potential could not be readily clamped for some of the less physiological voltage steps, the relevant points were excluded from data analysis. A scaled action potential waveform (FWHM=3.5ms, -70mV to +30mV) recorded from cultured hippocampal neuron was included before each step to estimate the fluorescence change of the indicators to action potential waveform. The kinetics of ASAP variants were calculated from voltage imaging data recorded at 800Hz camera frame rates in room-temperature. The ASAP expressing HEK293A cells were patched in a whole-cell voltage clamp mode and was given a pulse protocol to command the membrane potential change. The fluorescence response to a 100-mV step pulse was fitted to a mono-exponential function for both onset (depolarization) and offset (repolarization) segments to determine the relevant time constants.

To test ASAP variants' responses to simulated AP-shaped waveforms, a spontaneous spike with 100-mV amplitude recorded from a cultured hippocampal neuron was modified to have either 2ms or 4ms full-width at half-maximal (FWHM) and used as a command voltage for the HEK293A cells expressing ASAP variants. The fluorescence images were acquired at 800Hz.

Whole Cell Patch-Clamping and Imaging of Cultured Hippocampal Neurons

Cultured rat hippocampal neurons were transfected as described above with plasmids expressing ASAP6-Kv under the hSyn promoter. Patch-clamp electrophysiology was then performed 2–4 days post-transfection which was usually conducted on DIV 11–14. A coverslip with cultured neurons was kept in a patch chamber on the stage of Axiovert 100M inverted microscope (Zeiss), and were continuously perfused with ASCF solution (125 mM NaCl, 2.5 mM KCl, 2 mM $CaCl_2$, 1 mM $MgCl_2$, 25mM $NaHCO_3$, 1.25mM NaH_2PO_4, 15mM D(+) Glucose, Osmolarity: 300-305 mOsm) bubbled with carbogen gas (95% oxygen and 5% carbon dioxide) at room temperature. Patch pipettes were filled with 135 mM KCH_3SO_3, 8.1 mM KCl, 10 mM HEPES, 8 mM Na2-phosphocreatine, 0.3 mM Na_2GTP, 4 mM MgATP, 0.1 mM $CaCl_2$ and 1 mM EGTA, and the pH was adjusted to 7.2– 7.3 with osmolarity 285–290 mOsm. Action potentials were recorded in whole-cell current clamp mode with < 20pA holding current level. The APs were then evoked by injecting 500-ms long pulses with 50–250 pA amplitudes (50pA increment per pulse). The fluorescence images were captured at either 800 or 877 Hz using the iXon 860 EMCCD. Only the neurons with resting membrane potential less than −50 mV, R_a less than 17 MΩ, and R_m values with at least 10-fold greater than the R_a were analyzed. Fluorescence traces were corrected for photobleaching and

normalized to baseline by using custom codes in MATLAB as previously described[1], then exported to Excel (Microsoft) for graphing.

One-photon voltage imaging in retina

Murine retinal viral administration and explant dissection were conducted on intact flat-mounted retinas, following previously described protocols [15, 16]. Briefly, animals were anesthetized with 3% isoflurane. An incision was made in the sclera near the lens using a 30-gauge needle. Through this opening, 2 µl of AAV packaged with hSyn-ASAP6.1-Kv or hSyn-ASAP6b-Kv was injected into the subretinal space using a 5 µl Hamilton syringe held by a micromanipulator. A minimum incubation period of 21 days was observed before conducting experiments.

AAV-transduced retinas from male and female C57BL/6J mice (6–7 weeks old) were isolated in Ringer's medium (110 mM NaCl, 2.5 mM KCl, 1 mM $CaCl_2$, 1.6 mM $MgCl_2$, 10 mM D-glucose, and 22 mM $NaHCO_3$, bubbled with 5% CO_2/95% O_2). During the experiment, the tissue was superfused in Ringer's medium at 36°C and mounted ganglion-cell-side up on a piece of filter paper (MF-membrane, Millipore) with a 4.5 mm² opening in the center.

For 1-photon excitation and camera-based imaging of ASAP6 in the murine retina, samples were illuminated by a 50 mW/mm² beam from a 488 nm Obis laser (Coherent). The beam was controlled temporally using an acousto-optic modulator (Gooch and Housego), collimated, and passed through an iris mounted on an x-y stage. The iris was reimaged into the sample via the fluorescence excitation pathway, with fluorescence and excitation light separated using a Beamsplitter HC 495 dichroic (Semrock FF495-Di03-25x36). The size and position of the iris controlled the excitation spot diameter. Emission was imaged onto an ORCA Lightning camera (Hamamatsu) at a 1 kHz sampling rate. All images of ASAP6 fluorescence were quantified as counts per pixel per frame following supervised segmentation. The SNR was defined as the ratio of the mean fluorescence changes within ROIs, segmented cells, to the noise. The signal was calculated as the mean fluorescence intensity per pixel per frame within the ROI. The noise was defined as the standard deviation of the fluorescence intensity in the ROI during a baseline period, when no changes in fluorescence were measured. Spikes were detected using a simple function that identified peaks in the data based on convolution with a kernel and a threshold.

One-photon voltage imaging in motor cortex

Surgery and viral injection

To prepare mice for one-photon *in vivo* imaging from primary motor cortex, we followed the procedure previously described[1, 17] with a few modifications. Briefly, 8–9 weeks old male wild-type C57BL/6J mice (Jackson Laboratories, No. 000664) were injected with relevant GEVI viruses (AAV9-EF1a-DIO-ASAP6.1-Kv-WPRE (9.7x10^^{12} vg/mL) or AAV9-EF1a-DIO-ASAP6b-Kv-WPRE (1.1x10^^{13} vg/mL)) mixed with diluted CaMKIIα Cre virus (2.9×10^{13} GC/mL, Addgene #105558). All the GEVI viruses were produced by the Stanford GVVC. For each mouse, 450 nL of the GEVI virus was mixed with 50 nL of CaMKIIα Cre virus pre-diluted to make the GEVI virus (floxed) to diluted CaMKIIα Cre virus ratio to be either 314:1 (ASAP6.1-Kv) or 172:1 (ASAP6b-Kv) in terms of virus particles. The intracranial virus injection was done on the left hemisphere at the coordinate; ML –1.5 mm, AP 1.0 mm, and DV 1.2 –1.0 mm (all measured from bregma), for sparse labeling of layer 2/3 pyramidal neurons in motor cortex. Cranial window surgery was done after the injection. In brief, a 3×3-mm craniotomy was cut using #11 scalpel blades (Fine Science Tools) and a square coverslip (#1 coverslip glass, Warner Instruments) was implanted on top of the dura within the craniotomy with mild compression of the brain. The window was centered at ML –2.0 mm, AP 0.5 mm. The window was sealed to the skull using dental cement (C&B Metabond, Parkell) and at the end of surgery, a custom titanium headplate was attached to the skull to fixate the head to the microscope stage during subsequent imaging.

One-photon *in vivo* imaging and analysis

The 1-photon wide-field voltage imaging setup was similar to what was previously described[1]. Briefly, a BX-51 microscope (Olympus) equipped with a 470-nm LED (SOLIS-470C, Thorlabs), a long-working distance 20x objective lens (NA 1.0, Olympus), a Flash4.0 V2 scientific CMOS (sCMOS) camera

(C11440-22CA, Hamamatsu), and a FITC-5050A filter set (Semrock) was used. High-speed acquisition of fluorescence images at 500 fps was achieved by reading 64 vertical lines from the 4×4-binned sCMOS sensor. Light intensity was 40-50 mW/mm^2. Resulting images were converted to TIF files and corrected for lateral motion using turboReg[18]. The ROIs for neurons and background were selected using a customized program in MATLAB (Mathworks). Then the fluorescence trace was extracted from the TIF files, background-subtracted, and photobleach-corrected for spike detection and quantification in customized Python program. To correct for photobleaching, a piece-wise step function with 0.5-s window size was used to fit the fluorescence trace to estimate the baseline. In each 0.5-s window, the baseline was the average of the 30–80 percentile of the fluorescence values, to exclude extreme values and signals. Spike location was determined using the spikepursuit algorithm in VolPy[19]. For brightness comparison, background subtracted fluorescence intensity during the first second of each cellular ROI was averaged over time and compared. For SNR comparison, the noise was estimated by the standard deviation of the 20 Hz-high-pass-filtered and spike-removed trace, to exclude supra- and sub-threshold activities in the recording, and the signal was defined by the peak value of the spikes.

Two-photon *in vivo* imaging in barrel cortex

Surgery and Viral Injection

Mice aged two to three months old were anesthetized with isoflurane (1.0–1.5% in O2). C1, C2 and C3 whisker columns were localized using transcranial intrinsic signal optical imaging to target the viral injections. A 3-mm diameter craniotomy was made centered on the C2 column[20]. AA9-hSyn-ASAP6-kv was injected at 5–6 locations surrounding the C2 column at 250 µm and 350 µm depth. A chronic cranial window (3-mm diameter glass coverslip, #1 thickness, CS-3R, Warner Instrument) was attached with dental cement after viral injections. Before surgery, mice received dexamethasone (2 mg/kg), enrofloxican (5 mg/kg), and meloxicam (10 mg/kg). Buprenorphine (0.1 mg/kg) was administered as the post-operative analgesic.

Stimulus Delivery

At the start of each imaging session, mice were placed under light anesthesia with isoflurane and head-fixed under the 2-photon microscope. 9 whiskers (rows B-D, arcs 1-3) were inserted into a 3×3 array of small tubes with calibrated piezoelectric actuators, centered on the C2 whisker. Trials consisted of single 1×250-µm or trains of 5×150-µm whisker deflections that were applied 5 mm from the face with 100-ms spacing between stimuli within a train. Whisker stimuli were delivered in random order with equal probability. An inter-trial interval of 1.5 ± 0.5 s was used between trials. Approximately 80 trials were delivered over the course of 15 minutes imaging. Paw guards prevented paw contact with the piezos. Imaging experiments were performed in total darkness. Uniform white noise was continuously applied to mask sounds from piezo actuators. Stimulus delivery was controlled by an Arduino Mega 2560 and custom routines in Igor Pro (WaveMetrics).

Two photon imaging

2-photon imaging took place 3–4 weeks after viral injection on awake head-fixed mice. Imaging was performed with a modified, commercially available (ThorLabs) two-photon microscope[21]. A titanium-sapphire laser (Chameleon Ultra II, Coherent) was used as the two-photon excitation source, and a wavelength of 960 nm was used to excite ASAP6-Kv. A post-objective power of 30–50 mW was used for imaging at depths of 160–200 µm below brain surface. 192×64-pixel or 96 x 64-pixel fields of view were imaged using a pixel size of 0.694 µm per pixel or 0.798 µm per pixel, resulting in a 133 x 34 µm or 77 x 52 µm area, respectively, imaged at 220 fps.

Image Processing

Fluorescence images were corrected for x-y motion using NoRMCorre[22]. Neuronal regions-of-interests (ROIs) were manually annotated using ImageJ (NIH) based on the mean intensity image. $\Delta F/F_0$ traces were extracted, with F_0 defined as the mode of the fluorescence histogram of the ROI across each 15-minute movie. Spike locations and subthreshold activity was extracted using the CaImAn algorithm[19] and custom Python routines (available at the SpkXtract Github repository) unless otherwise stated.

REFERENCES

1. Evans, S. W. *et al.* A positively tuned voltage indicator for extended electrical recordings in the brain. *Nat Methods* **20**, 1104–1113 (2023).
2. Villette, V. *et al.* Ultrafast Two-Photon Imaging of a High-Gain Voltage Indicator in Awake Behaving Mice. *Cell* **179**, 1590–1608.e23 (2019).
3. Chamberland, S. *et al.* Fast two-photon imaging of subcellular voltage dynamics in neuronal tissue with genetically encoded indicators. *Elife* **6**, e25690 (2017).
4. Horn, R. Uncooperative voltage sensors. *J Gen Physiol* **133**, 463–466 (2009).
5. Dana, H. *et al.* Sensitive red protein calcium indicators for imaging neural activity. *Elife* **5**, e12727 (2016).
6. Helmchen, F., Borst, J. G. & Sakmann, B. Calcium dynamics associated with a single action potential in a CNS presynaptic terminal. *Biophys J* **72**, 1458–1471 (1997).
7. Koester, H. J. & Sakmann, B. Calcium dynamics associated with action potentials in single nerve terminals of pyramidal cells in layer 2/3 of the young rat neocortex. *J Physiol* **529 Pt 3**, 625–646 (2000).
8. Liu, Z. *et al.* Sustained deep-tissue voltage recording using a fast indicator evolved for two-photon microscopy. *Cell* **185**, 3408–3425.e29 (2022).
9. Abdelfattah, A. S. *et al.* A general approach to engineer positive-going eFRET voltage indicators. *Nat Commun* **11**, 3444 (2020).
10. Shuman, T. *et al.* Breakdown of spatial coding and interneuron synchronization in epileptic mice. *Nat Neurosci* **23**, 229–238 (2020).
11. Ghosh, K. K. *et al.* Miniaturized integration of a fluorescence microscope. *Nat Methods* **8**, 871–878 (2011).
12. Cai, D. J. *et al.* A shared neural ensemble links distinct contextual memories encoded close in time. *Nature* **534**, 115–118 (2016).
13. Lam, A. J. *et al.* Improving FRET dynamic range with bright green and red fluorescent proteins. *Nat Methods* **9**, 1005–1012 (2012).
14. Baker, C. A., Elyada, Y. M., Parra, A. & Bolton, M. M. Cellular resolution circuit mapping with temporal-focused excitation of soma-targeted channelrhodopsin. *Elife* **5**, e14193 (2016).
15. Busskamp, V. *et al.* Genetic reactivation of cone photoreceptors restores visual responses in retinitis pigmentosa. *Science* **329**, 413–417 (2010).
16. Drinnenberg, A. *et al.* How Diverse Retinal Functions Arise from Feedback at the First Visual Synapse. *Neuron* **99**, 117–134.e11 (2018).
17. Hwang, F. J. *et al.* Motor learning selectively strengthens cortical and striatal synapses of motor engram neurons. *Neuron* **110**, 2790–2801.e5 (2022).
18. Thévenaz, P., Ruttimann, U. E. & Unser, M. A pyramid approach to subpixel registration based on intensity. *IEEE Trans Image Process* **7**, 27–41 (1998).
19. Cai, C. *et al.* VolPy: Automated and scalable analysis pipelines for voltage imaging datasets. *PLoS Comput Biol* **17**, e1008806 (2021).
20. Drew, P. J. & Feldman, D. E. Intrinsic signal imaging of deprivation-induced contraction of whisker representations in rat somatosensory cortex. *Cereb Cortex* **19**, 331–348 (2009).
21. Fan, J. L. *et al.* High-speed volumetric two-photon fluorescence imaging of neurovascular dynamics. *Nat Commun* **11**, 6020 (2020).
22. Pnevmatikakis, E. A. & Giovannucci, A. NoRMCorre: An online algorithm for piecewise rigid motion correction of calcium imaging data. *J Neurosci Methods* **291**, 83–94 (2017).